The effects of transverse prestressing on the shear and bond behaviors of R/C columns

Y. Shinohara
Structural Engineering Research Center, Tokyo Institute of Technology, Tokyo, Japan

H. Watanabe
Department of Architecture, Nagasaki Institute of Applied Science, Nagasaki, Japan

ABSTRACT: Experiments and 3-D FEM analyses were performed on reinforced concrete columns laterally prestressed by the shear reinforcement to study the influence of the active confinement upon shear crack behaviors and bond splitting strength. Many strain gauges were attached to main bars and hoops, and the width of each crack over transverse hoops was measured by a digital microscope. Transverse prestressing increases the bond splitting strength as well as the shear capacity at first cracking and the ultimate shear strength, and decreases the width values of cracks. The FEM analyses can evaluate the shear capacity at first cracking, ultimate shear strength and the bond splitting strength with a fair degree of precision, and provide valuable information about the effect of the active confinement on shear and bond behaviors by evaluating the intensity of confinement in tri-axial state of stress with minimum principal stress and equivalent confining pressure.

1 INTRODUCTION

Prestressing in concrete structures is generally aimed at controlling the flexural cracks by the arrangement of tendons in an axial direction of any given member. On the other hand, in order to delay the onset of shear cracking and to reduce its width, not to control a flexural crack, experimental studies have been conducted on the reinforced concrete (RC) columns laterally prestressed by the shear reinforcement with high strength (Watanabe et al. 2004). The results of the flexure-shear tests have indicated that the shear capacity at first diagonal cracking is increased and the width values of shear cracks, especially their residual opening are remarkably reduced by transverse prestressing. This reduction of the crack opening has improved not only durability but also earthquake resistance since the ability to transmit shear force across a rough crack increases dramatically by reducing its width (Shinohara et al. 1999). The three dimensional finite element (FEM) analyses were also performed on RC columns mentioned above to investigate the effect of the lateral confinement using the equivalent confining pressure and the degree of damage in compressive zone as the gauges that evaluate active confinement and compressive-shear failure quantitatively (Shinohara et al. 2004). These studies have revealed that an increase in the resistance against shear failure as well as shear cracking with increasing prestress in the shear reinforcement could be explained by the triaxial state of stress in the core concrete.

The primary purpose of this study is to investigate how transverse prestressing in RC columns would affect the shear behaviors and bond behaviors on the basis of the triaxial state of stress, to clarify the relationship between the width of a shear crack and the strain of a shear reinforcement, and to see the extent to which the FEM analysis with a smeared crack model and a bond-slip model can evaluate the actual shear crack behavior and the bond strength.

2 OUTLINE OF TEST AND ANALYSIS

2.1 *Test specimens*

The details of the test specimen are shown in Figure 1. The main characteristics of the specimens are summarized in Table 1. The flexure-shear tests have been performed on four columns which were laterally prestressed (LPRC) and not prestressed (RC). The specimens were designed to cause a shear failure before the longitudinal reinforcement yield by Architectural Institute of Japan (1999). Two columns of them (B-series) were designed to cause a bond failure first by removing reinforcement (D13 in Fig. 1) that prevent bond splitting failures. The test specimens had a square cross section of 340 mm x 340 mm and a height of 900 mm. The lateral prestress was introduced into concrete as follows: (1) the high strength transverse hoops (U6.4 in Fig. 1) were pretensioned to about 40% of the yield stress using the rigid steel molds and special jigs shown in Figure 1, (2) concrete was vertically placed into the molds and cured until the strength of concrete increased adequately, (3) the core concrete was laterally prestressed by removing the steel molds. The product of the ratio (p_w) and the stress (σ_{wp}) of the pretensioned transverse reinforcement is defined as average lateral prestress σ_L ($=p_w\sigma_{wp}$) to indicate the intensity of lateral prestress. The mix proportion of concrete used in the test specimens is given in Table 2. The coarse aggregate used in the mix is natural round sea gravel with a maximum aggregate size of 25 mm. The bond splitting and shear strength are calculated in accordance with AIJ design guideline (1999) and other researchers, summarized in Table 3. The effect of transverse prestressing on bond splitting strength is counted by adding the average prestress to the tensile strength of concrete.

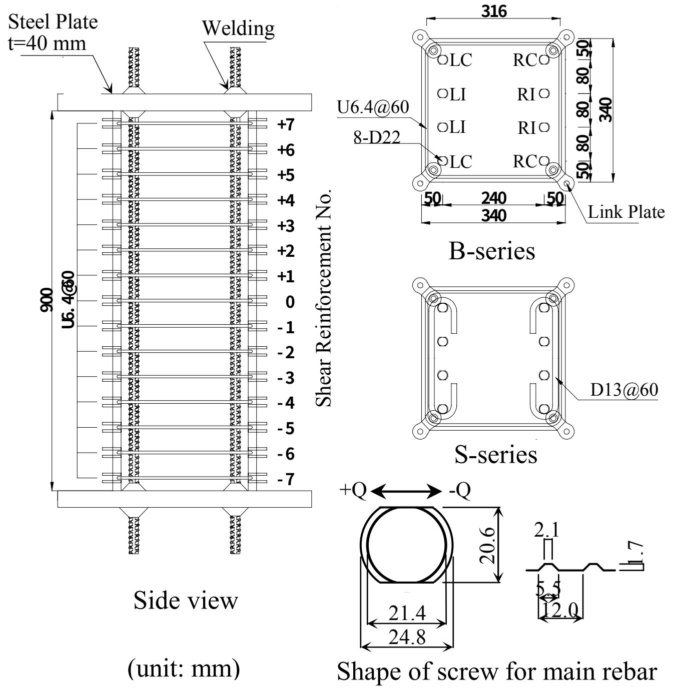

Figure 1. Details of test specimen and reinforcement.

Table 1. List of test specimens.

Test	M/QD	p_w	p_{wb}	σ_B	σ_{wp}	σ_L
Series		%			N/mm^2	
B-RC	1.3	0.29	0.29	47.7	0	0
B-LPRC	1.3	0.29	0.29	47.1	587	1.7
S-RC	1.3	0.29	1.54	50.8	0	0
S-LPRC	1.3	0.29	1.54	46.5	536	1.6

M / QD=shear span-depth ratio, p_w=ratio of transverse hoop, p_{wb}=ratio of transverse reinforcement including hook against bond split, σ_B=compressive strength of concrete, σ_{wp}=introduced prestress in transverse hoop, σ_L=lateral prestress ($=p_w\sigma_{wp}$)

Table 2. Mix Proportion.

Proportion, by weight				Admixture	Slump
Cement	Sand	Gravel	Water	Super	cm
1	2.04	2.53	0.5	plasticizer	21

Table 3. Bond splitting strength and shear strength.

Test	Bond strength N/mm^2			Q_{bu}F	Q_{bu}M	Q_{bu}D	${}_{cal}Q_{sc}$	${}_{cal}Q_{su}$
Series	τ_{bu}F	τ_{bu}M	τ_{bu}D			kN		
B-RC	4.2	5.4	3.4	445	511	399	470	629
B-LPRC	5.9	7.1	5.1	580	647	536	612	730
S-RC	-	-	8.7	-	-	694	496	648
S-LPRC	-	-	10.1	-	-	809	606	725

τ_{bu}F=τ_{bu} by Fujii (1983), τ_{bu}M=τ_{bu} by Maeda (1994), τ_{bu}D=τ_{bu} by AIJ Design guidelines (1999), Q_{bu}F, Q_{bu}M and Q_{bu}D = shear strength using τ_{bu}F, τ_{bu}M and τ_{bu}D ${}_{cal}Q_{sc}$, ${}_{cal}Q_{su}$ =shear crack and ultimate strength by Watanabe (2004)

2.2 *Test set-up and instrumentation*

The loading apparatus is shown in Figure 2. The vertical force on the test specimen was supplied by the 2 MN-hydraulic jack, and the ratio of axial load to axial strength was kept constant at 0.3 during a test. The horizontal force was supplied by two hydraulic jacks with the capacity of 500 kN, and controlled in displacement. The cyclic horizontal load was applied in the way to produce an antisymmetric moment in a column. The horizontal load was turned back when the rotation angle of member, *R* reached ±1/400, ±1/200, ±1/133 (B-series only), ±1/100, ±1/67, ±1/50 and ±1/33, until after the peak load. The width of each shear crack close to the shear reinforcement was measured using two digital microscopes with a resolution of 0.01 mm every cycle three times in loading and two times in unloading. The crack width used in this paper is defined as a distance normal to the direction of a crack, as illustrated in Figure 3. Three strain gauges were glued on each leg of all transverse hoops, and their locations and designations are shown in Figure 3. Seven strain gauges were also glued on each longitudinal reinforcement of B-series specimens to evaluate the bond stress.

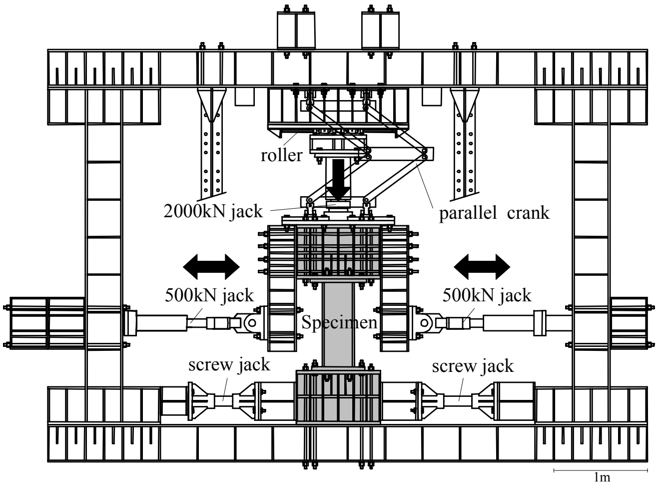

Figure 2. Loading apparatus and test specimen.

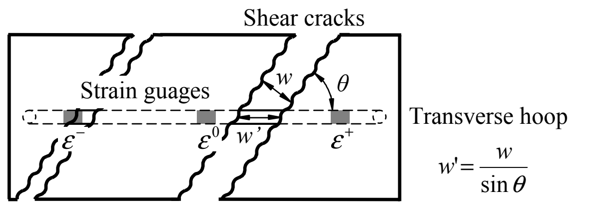

Figure 3. Definition of crack width and designations of three strain gauges.

2.3 *Analytical models and idealizations*

The finite element mesh and boundary condition of the analytical model are shown in Figure 4. The mechanical properties of concrete and reinforcement are shown in Figure 5 and 6 together with their idealizations in analyses. Due to the symmetry, only one half of the column was analyzed. The stiff elements were attached at the top and bottom of a column to idealize steel stubs. The top nodes were constrained to move uniformly in the vertical direction and not to allow the upper stiff elements to rotate, so that a column deformed in an antisymmetric mode. The bond-slip between concrete and reinforcement was not considered in analysis of S-series because an additional reinforcement was installed to avoid a bond splitting failure. On the other hand, the bond-slip relation shown in Figure 7 was assumed in analysis of B-series. When loading, the prescribed prestress was first introduced into the shear reinforcement, and then the axial load was applied in load control, finally the shear load was applied in displacement control. The maximum-tensile-stress criterion of Rankine was adopted as a failure criterion in the tension zone of concrete. Smeared cracking and bilinear tension softening shown in Figure 5 are adopted in this analysis. The shear stiffness of cracked concrete is generally dependent on the crack width. This phenomenon is taken into account by decreasing the shear stiffness with an increase of the normal crack strain. Drucker-Prager criterion was used for a failure criterion in the compressive zone of concrete. The formulation is given by

$$f(I_1, J_2) = \alpha I_1 + \sqrt{J_2} - k = 0 \tag{1}$$

$$\alpha = \frac{2\sin\phi}{\sqrt{3}(3-\sin\phi)} \tag{2}$$

$$k = \frac{6\cos\phi}{\sqrt{3}(3-\sin\phi)}c \tag{3}$$

$$I_1 = \sigma_1 + \sigma_2 + \sigma_3 \tag{4}$$

$$J_2 = \left[(\sigma_1-\sigma_2)^2 + (\sigma_2-\sigma_3)^2 + (\sigma_3-\sigma_1)^2\right]/6 \tag{5}$$

Where φ is the internal-friction angle, c is the cohesion; σ_1, σ_2 and σ_3 are the principal stresses (see Chen 1982). The internal-friction angle of Drucker-Prager was determined based on experimental results performed on concrete cylinders with different strengths and hoops to study the effect of lateral confinement by Takamori et al. (1996). According to their test results, the strength of concrete confined by lateral reinforcement similar to our specimen increases to (σ_B+2.0σ), where σ_B is the compressive strength of plain concrete and σ is the averaged lateral confining stress. An increasing rate of 2.0 to σ is under half 4.1 proposed by Richart (1928) due to the partial confinement by hoops. From this equation, a set of principal stresses that corresponds to the

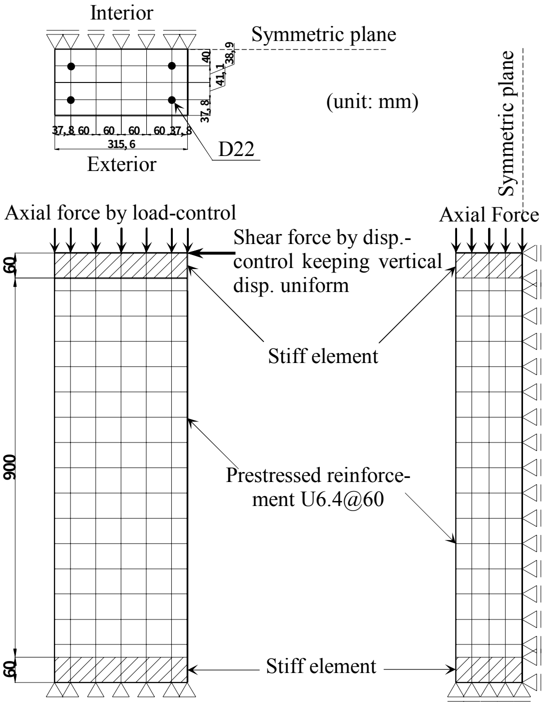

Figure 4. Details of finite element model of B-series.

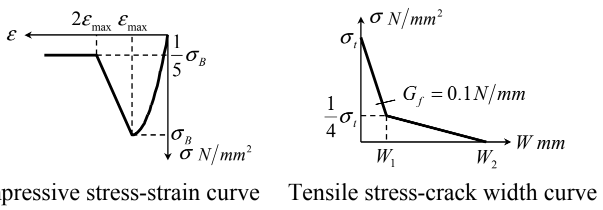

Test Series	σ_B N/mm²	ε_{max} %	E_c N/mm²	σ_t N/mm²	W_1 mm	W_2 mm
B-RC	47.7	-0.2	3.38E+4	3.0	0.030	0.15
B-LPRC	47.1	-0.2	3.56E+4	3.0	0.030	0.15
S-RC	50.8	-0.2	3.51E+4	2.9	0.031	0.15
S-LPRC	46.5	-0.2	3.45E+4	2.9	0.031	0.15

Poisson's ratio ν=0.2

Figure 5. Mechanical properties and idealizations for concrete.

Bar Type	σ_y (N/mm²)	σ_{max} (N/mm²)	E_s (N/mm²)
D22	1196	1281	1.92E+5
U6.4	1459	1499	2.04E+5
D13	344	488	1.92E+5

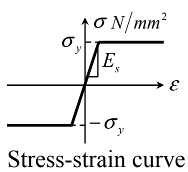

Figure 6. Mechanical properties and idealizations for rebars.

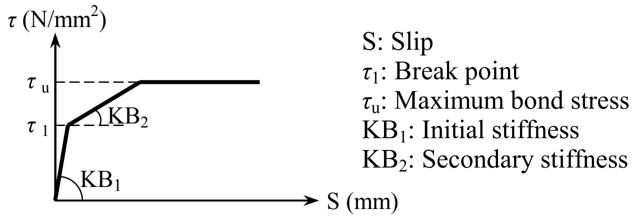

Test Series	Bar Position	KB_1 (N/mm³)	KB_2 (N/mm³)	τ_1 (N/mm²)	τ_u (N/mm²)
B-RC	Corner	88.2	5.88	1.76	4.95
B-RC	Intermediate	88.2	5.88	1.76	4.24
B-LPRC	Corner	88.2	5.88	1.76	7.88
B-LPRC	Intermediate	88.2	5.88	1.76	5.41

Figure 7. Analytical model for bond-slip relationship.

strength of concrete in a triaxial state of stress with confining pressure is determined as: $\sigma_1=\sigma_2= -\sigma$, $\sigma_3= -(\sigma_B+2.0\sigma)$. The minus refers to compression. By substituting these principal stresses into Equation 1

$$f(I_1, J_2) = (1-\sqrt{3}\alpha)\sigma_B + (1-4\sqrt{3}\alpha)\sigma - \sqrt{3}k = 0 \tag{6}$$

Because Takamori's tests (1996) showed a constant coefficient of 2.0 for any value of the averaged confining stress, Equation 6 must be valid regardless of σ, as well. Therefore, the multiplication factor of second term in Equation 6 must be zero:

$$(1-4\sqrt{3}\alpha) = 0 \quad \Rightarrow \quad \alpha = \frac{1}{4\sqrt{3}} \tag{7}$$

By substituting Equation 7 into Equation 2, the internal-friction angle of 20º is estimated to be suitable for triaxial state of stress confined laterally by reinforcement in a similar way to this specimen.

3 RELATION BETWEEN SHEAR BEAHAVIOR AND LATERAL CONFINEMENT

3.1 *Shear load-rotation angle curves*

The shear load Q-rotation angle R curves obtained from the tests of B-series and S-series are shown for comparison in Figure 8, and figure 9 shows Q-R curves, compared with the results of analysis. For the typical crack behavior observed during S-series tests, flexural cracks appeared first, and they extended into flexural shear cracks near the both end of the specimen, and finally shear cracks occurred with increasing shear load. The maximum shear loads for S-RC and S-LPRC were 617 kN when R=1/100 and 762 kN when R=1/67 respectively. The shear loads for both S-RC and S-LPRC were gradually reduced without any reinforcement's yielding by crushing concrete in the compressive zone at the top and bottom ends. For B-series specimens designed to cause bond failure, on the other hand, the maximum shear loads were 25 % lower than those of S-series due to the bond splitting, and the stiffnesses deteriorated slightly to reach the peak loads at R=1/67. The flexural cracks for both B-RC and B-LPRC column appeared first at R=1/200. The bond splitting cracks in B-RC were observed at R=1/133 and extended over the longitudinal reinforcement with sequent loading cycles. For B-LPRC, the shear cracks preceded the bond splitting cracks when R=1/100 at the bottom of specimen and extended along the longitudinal reinforcement. The shear cracking, bond splitting and ultimate shear strength obtained from experiments and FEM analyses are compared in Table 4. The shear capacity at first cracking provided by the analysis is defined as the shear load which causes a strain in shear reinforcement to increase rapidly. Compared with the bond strength in Table 3, the test results are 10% higher than AIJ design guidelines (1999) and 10% lower than Maeda's equation (1994). It should be noted that the longitudinal rebars are not directly supported by transverse rebars (see Fig. 1) and this may reduce the effect that controls bond splitting.

As for S-series tests, the relations between shear crack stress $_{exp}\tau_{sc}$ (=$_{exp}Q_{sc}/bD$) and lateral prestress, and between ultimate shear stress $_{exp}\tau_{su}$ (=$_{exp}Q_{su}/bD$) and lateral prestress are plotted in Figure 10 together with Watanabe's data (2004) marked by solid-white (σ_B=35 N/mm^2). The difference in strength of concrete was adjusted by dividing them by the characteristic strength to determine their failure modes. It can be seen from Figure 10 that the shear crack and ultimate strength have increased proportionally with

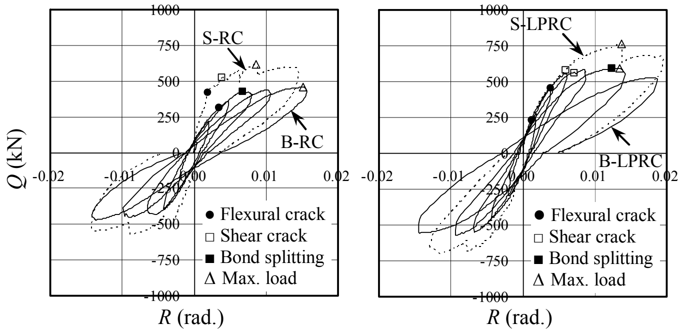

(1) RC nonprestressed (2) LPRC prestressed

Figure 8. Comparisons of Q-R between S series and B series specimens (Envelop curves for S-series).

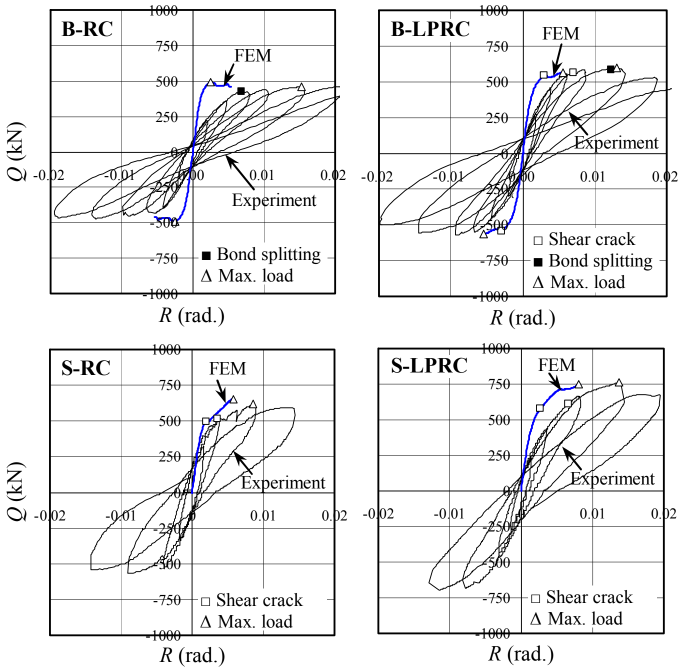

Figure 9. Comparisons between analytical and experimental Q-R curves.

Table 4. Shear cracking, bond splitting and ultimate strength.

Test Series	$_{exp}Q_{sc}$	$_{exp}Q_{bu}$	$_{exp}Q_{su}$	$_{FEM}Q_{sc}$	$_{FEM}Q_{bu}$	$_{FEM}Q_{su}$
	kN					
B-RC	-	461	-	-	493	-
B-LPRC	562	595	-	547	565	-
S-RC	515	-	617	495	-	655
S-LPRC	611	-	762	577	-	747

$_{exp}Q_{sc}$ and $_{FEM}Q_{sc}$ =shear capacity at first cracking by test and FEM
$_{exp}Q_{bu}$ and $_{FEM}Q_{bu}$ =bond splitting strength by test and FEM
$_{exp}Q_{su}$ and $_{FEM}Q_{su}$ =ultimate shear strength by test and FEM

increasing lateral pressure. Furthermore, Figure 11 shows a comparison of the shear strengths obtained from experiment and analysis in both test series. The predictions of FEM analysis are consistent with all existing experimental data for the shear capacity at first cracking and the ultimate shear strength.

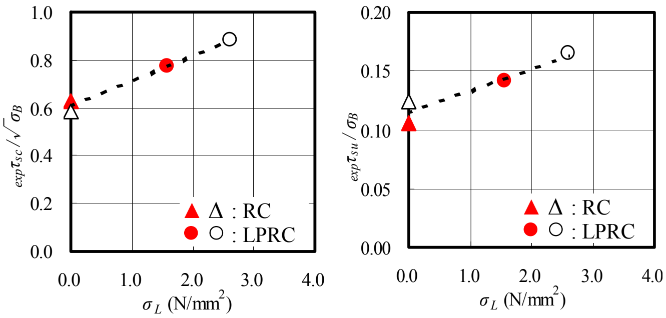

(1) Shear capacity at first cracking (2) Ultimate shear strength

Figure10. Increase of strength with increasing lateral prestress.

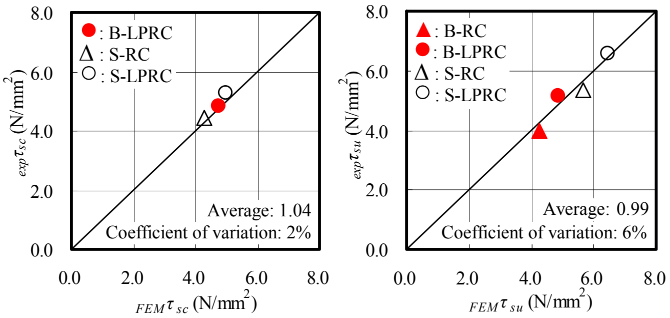

(1) Shear capacity at first cracking (2) Ultimate shear strength

Figure 11. Comparison of strength from experiment and FEM.

3.2 *Triaxial state of stress by FEM analysis*

The effect of the lateral confinement on the shear behavior is evaluated based on the triaxial state of stress in the concrete. Figure 12 shows the distributions of the minimum principal stress in the center of S-RC and S-LPRC specimens. For S-RC specimen, the compressive strut formed by a large compressive stress was revealed at the shear load of 550 kN, thereafter, the width of the strut reduced slightly and localized in a diagonal direction at the maximum load. For S-LPRC specimen, on the other hand, the compressive strut appeared at the shear load roughly similar to the maximum load of RC and the width of the strut increased gradually up to the maximum load. The degree of damage for compressive failures and the equivalent confining pressure were introduced as the gauges to evaluate the effect of active confinement on the stress state in the core concrete quantitatively, as shown in Figure 13. The degree of damage for compressive failures is defined using the deviated part of the stress state in principal stress space. Figure 14 shows the degree of damage for compressive failures in the surface of S-RC and S-LPRC specimens at the same shear load as Figure 12. It can be seen from Figure 12 and Figure 14 that the distributions of the degree of damage correspond roughly with those of the minimum principal stress. This degree of damage for S-LPRC is lowered compared with RC specimen. The red parts dotted with a white dot at the top and bottom ends represent the post-peak softening zone of concrete, so that the failure mode of analysis is quite similar to that of experiment. The post-peak softening of concrete for S-RC specimen occurred when the shear load is about 600 kN, and the softening zone was limited to the small area. This softening for S-LPRC specimen, on the contrary, occurred at the shear load of 700 kN, and the softening zone was gradually expanded up to the maximum load. The equivalent confining pressure is defined as the lateral pressure when converting the stress state on a random stress-path into that on the stress-path according to the triaxial compressive test with a constant lateral pressure, as shown in Figure 13. Consequently, the equivalent confining pressure increases with increasing hydrostatic component and decreasing deviated component of the stress state in principal stress space. The ratio of the equivalent confining pressure to the strength of concrete is shown in Figure 15 to compare S-RC with S-LPRC at maximum shear loads. As for S-LPRC specimen, the active confinement that is over ten times higher than the passive confinement was produced after applying the axial load, and it covered wider parts of the specimen than RC specimen until the maximum shear load.

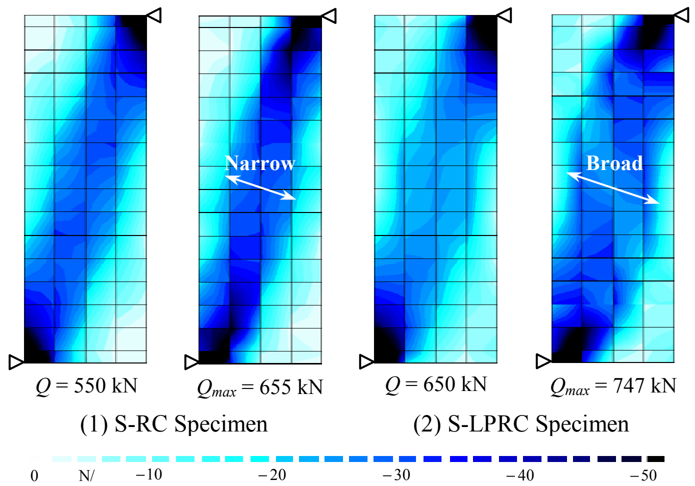

Figure 12. Compression strut based on minimum principal stress.

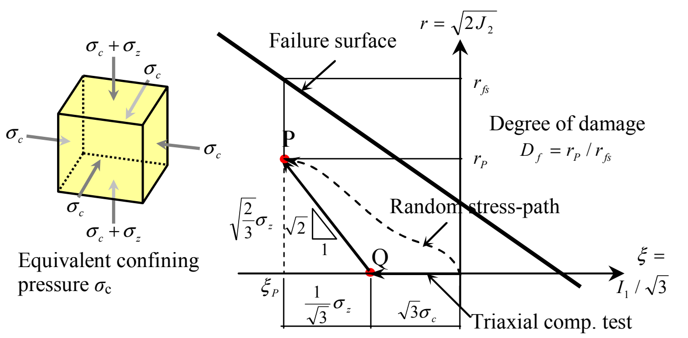

Figure 13. The degree of damage and equivalent confining pressure for triaxial state of stress in meridian plane of Drucker-Prager criterion.

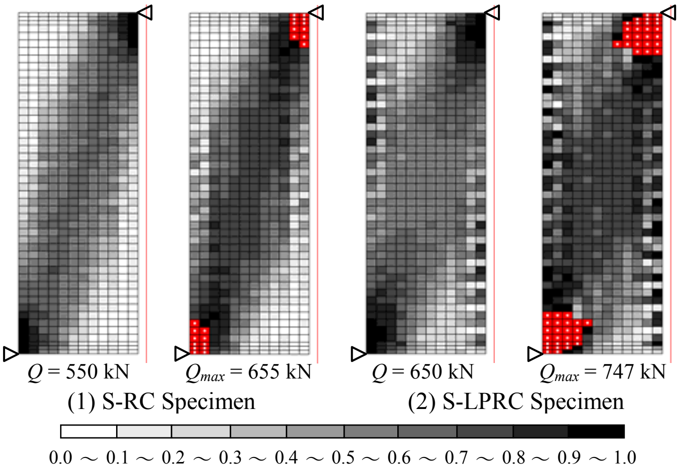

Figure 14. Comparison of damage in compression zone.

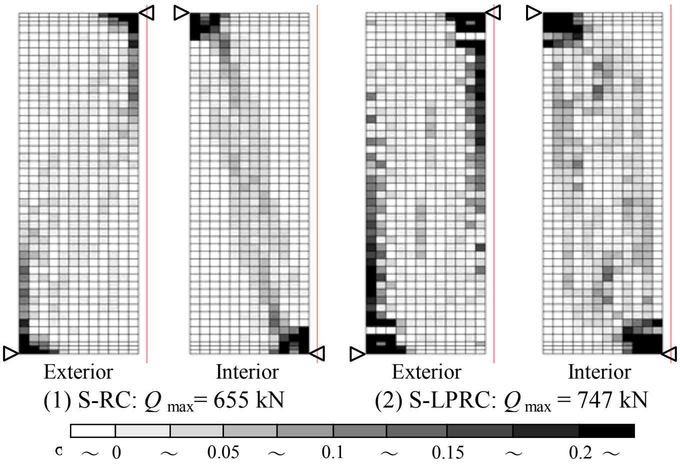

Figure 15. Comparison of equivalent confining pressure at maximum shear load of S-series specimens.

4 SHEAR CRACK BEHAVIOR

4.1 *Shear crack patterns*

Figure 16 shows the contours of the crack strain obtained by analyses and the diagrams of shear cracks observed by S-series tests. The lateral confinement in S-LPRC specimen restrained greatly shear cracks from propagating at the shear load similar to the peak load of S-RC specimen, and the final crack pattern of S-LPRC differed drastically from that of S-RC. The shear cracks developed scatteringly in the upper and lower side of S-LPRC specimen, whereas they developed intensively in the center of S-RC specimen. The FEM analyses using smeared crack model cannot evaluate an individual crack but can detect the difference in crack patterns between S-RC and S-LPRC specimen.

Figure 17 shows the crack patterns observed in B-series and S-series tests at the maximum loads. Cracks with the width of 0.5 mm and over are emphasized using thick lines. In B-series columns, more bond splitting cracks appears along the longitudinal reinforcement and the crack angle is smaller than S-series columns. Small crack angle weakens the effect of shear reinforcement and brings wider cracks. The distributions of crack width over the transverse reinforcement where the total width of cracks is the largest are shown in Figure 18 to compare B-series with S-series. Transverse prestressing can disperse shear cracks along the depth of columns in S-series, whereas bond splitting cracks in B-series columns tend to concentrate near the longitudinal reinforcement regardless of the lateral prestress.

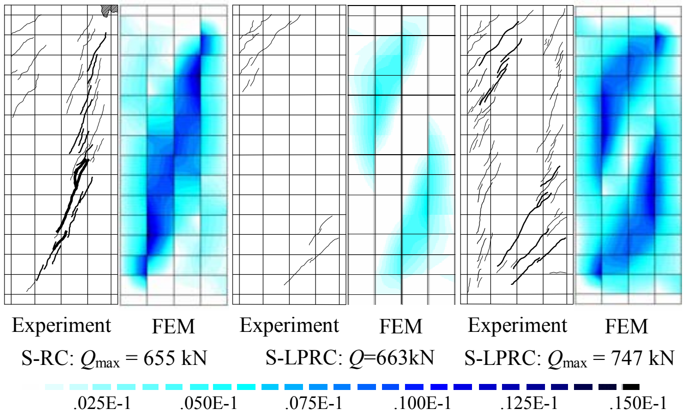

Figure 16. Crack patterns from experiment and crack strain from FEM analysis in S-series tests.

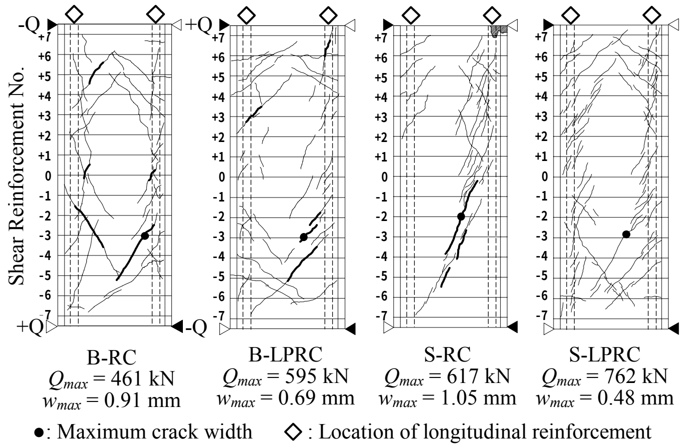

Figure 17. Crack patterns at maximum shear load.

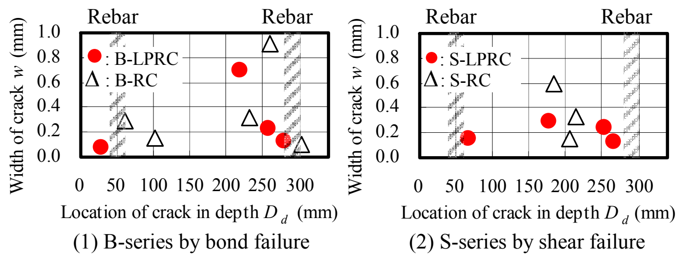

Figure 18. Width and distribution of shear crack.

4.2 *Estimations of shear damage by FEM analysis*

To investigate how accurate the FEM analysis with a smeared crack model can evaluate the extent of actual shear crack damage, the total crack width by FEM analysis, $\Sigma_{FEM}w$, which is estimated from the nodal displacements at both ends of a shear reinforcement by neglecting the strains of concrete, is shown in Figure 19 together with $\Sigma_{exp}w'$ by microscopes and $\Sigma_{cal}w$ calculated by integrating strains of hoops. Although $\Sigma_{exp}w'$ is observed on the surface of concrete while $\Sigma_{cal}w$ and $\Sigma_{FEM}w$ are estimated by a reinforcement, these three crack width values exhibit broadly similar behavior due to the small concrete cover of 9 mm. The difference between the crack width values of S-RC and S-LPRC specimen is basically consistent with that of shear crack behaviors shown in Figure 16 since the total crack width faithfully reflects their behaviors. Especially, the experimental and analytical crack width, $\Sigma_{cal}w$ and $\Sigma_{FEM}w$ are similar along the height of columns.

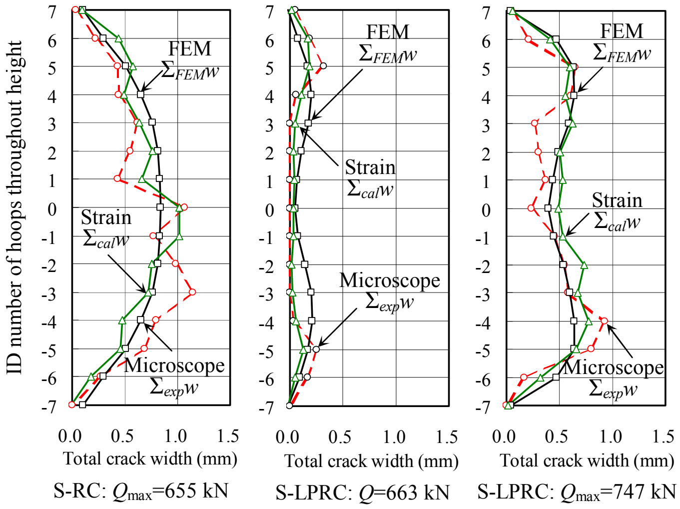

Figure 19. Plots of crack width measured by means of microscope and of strain in hoops, and comparison with analysis.

5 RELATION BETWEEN BOND BEAHAVIOR AND LATERAL CONFINEMENT

5.1 *Strains in longitudinal reinforcement*

The identification of longitudinal reinforcement and zonings divided by strain gauges to calculate bond stress is shown in Figure 20. After axial loading, compressive strain of each longitudinal rebar was about 300 to 400 μ and no bar yielded until shear loading was terminated. Figure 21 shows the distributions of strains in longitudinal reinforcement of B-series specimens, compared with the results of FEM analysis. The strains of tension zones damaged by shear cracks become constant as it called tension-shift. The analytical results of left rebars agree with the experimental data much better than those of right rebars. This is mainly because the experimental data of bond strength for left rebars are adopted in bond-slip relations. However, this analysis that considered only the bond strength cannot estimate the effect of lateral confinement on the bond stiffness and the difference between corner and intermediate rebars. It is necessary to improve further the analytical model.

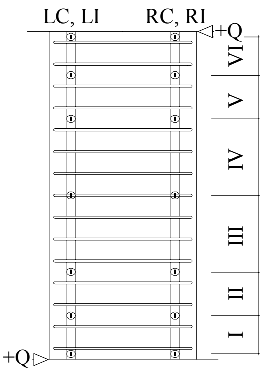

Rebar's ID
LC: Left-corner bar
LI : Left-intermediate bar
RC: Right-corner bar
RI : Right-intermediate bar
See Figure 1.

Figure 20. Identification of longitudinal reinforcement and zoning for bond stress.

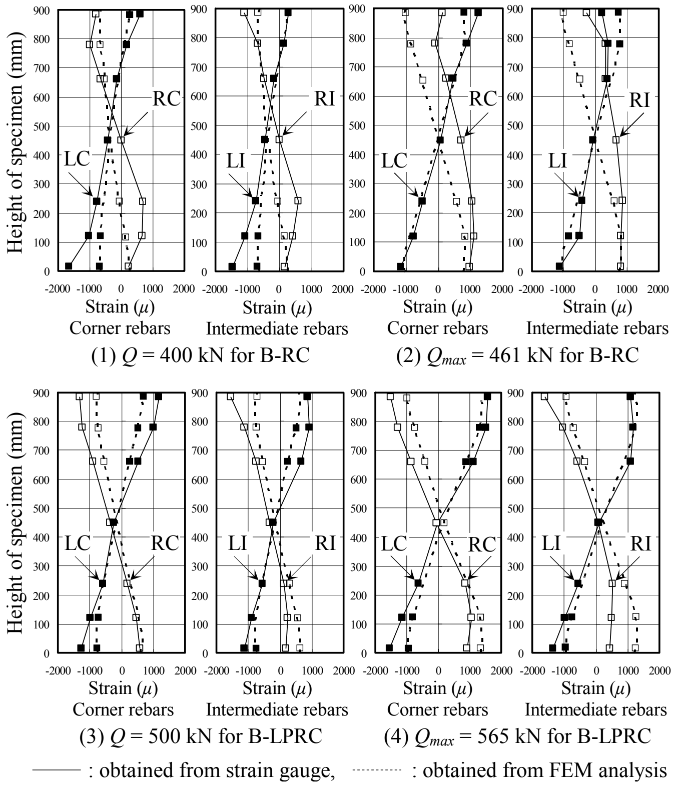

Figure 21. Strain distributions in longitudinal reinforcements.

5.2 *Bond behaviors in longitudinal reinforcement*

The local bond stress is defined as an average bond stress of zonings shown in Figure 20. The average bond stress is calculated by dividing the differential force between zonings by the product of the zone's length and rebar's perimeter. The relations between local bond stress τ_b and rotation angle R for left rebars in each zone are in Figure 22 where bold lines indicate corner bars and thin lines intermediate bars. Each local bond stress apart from two zones damaged by shear cracks is summarized in Table 5. The bond strength of corner rebars is higher than that of intermediate rebars and this trend is stronger for the compressive zones of B-LPRC (zone I and II). Figure 23 shows the relation between average bond stress of right rebars for zone III to VI and rotation angle. As can be predicted from the strain distributions in Figure 21, the bond stress of B-RC specimen decreases rapidly when bond cracks occurred at the shear load of 415 kN and less than half of the maximum bond stress at the peak shear load irrespective of the position of the rebar. The bond stress of B-LPRC specimen, on the other hand, retains most of the maximum bond stress until the peak shear load and decreases slowly after that. This reason is that transverse prestressing prevents the bond splitting crack along the longitudinal rebars from developing afterwards into a side splitting failure.

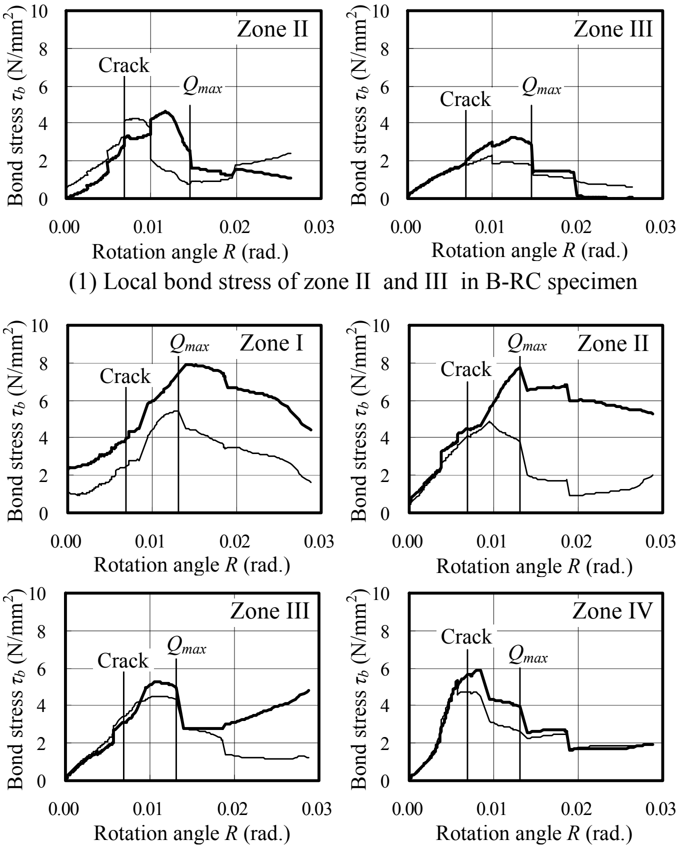

(2) Local bond stress of zone I to IV in B-LPRC specimen

Bold lines: Left-corner rebars (LC), Thin lines: Left-intermediate rebars (LI)

Figure 22. Relations between local bond stress of left side rebar and rotation angle.

Table 5. List of maximum local bond stress at each zone.

Test	Bar	Maximum local bond stress τ_b (N/mm^2)					
B-Series	ID	Zone I	Zone II	Zone III	Zone IV	Zone V	Zone VI
RC	LC	-	4.95	3.24	2.64	-	-
RC	LI	-	4.24	2.31	2.10	-	-
RC	RC	-	-	3.79	4.00	3.80	2.40
RC	RI	-	-	3.29	3.11	2.31	4.17
LPRC	LC	7.88	7.75	5.27	5.91	-	-
LPRC	LI	5.41	4.87	4.52	5.14	-	-
LPRC	RC	-	-	4.64	4.70	5.83	6.90
LPRC	RI	-	-	3.10	3.47	4.44	5.64

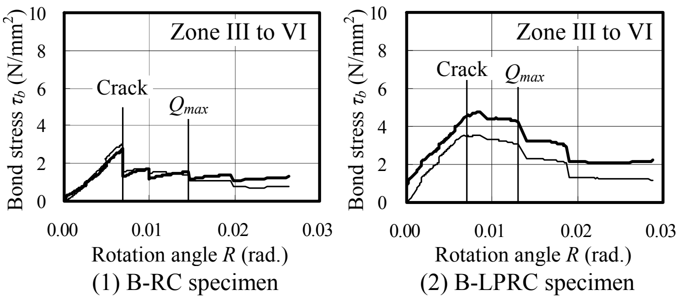

Bold lines: Right-corner rebars(RC), Thin lines: Right-intermediate rebars(RI)

Figure 23. Relations between average bond stress of right side rebar and rotation angle.

6 CONCLUSIONS

The following conclusions are obtained from experiments and 3-D FEM analyses performed on reinforced concrete columns laterally prestressed to investigate the effect of the active confinement upon shear and bond behaviors.

1) The shear capacity at first cracking and ultimate shear strength have increased proportionally with increasing lateral pressure.
2) The FEM analyses have revealed that an increase in resistance against shear failure as well as shear cracking with increasing lateral prestress could be explained by the triaxial state of stress in the core concrete.
3) The shear crack patterns have changed appreciably, and the spacing and width of cracks have decreased drastically by transverse prestressing.
4) The FEM analyses using smeared crack model cannot evaluate a localized crack accurately but can provide valuable information about the total damage along the depth of a column.
5) Removing reinforcement to prevent bond splitting failures reduces the ultimate shear strength by 25 % and leads to bond failure mode.
6) The FEM analyses using bond-slip model can evaluate the bond splitting strength and the distributed strains of longitudinal reinforcement.
7) The bond strength after cracking has been improved by transverse prestressing.

REFERENCE

Architectural Institute of Japan (1999). Design Guidelines for Earthquake Resistant Reinforced Concrete Buildings Based on Inelastic Displacement Concept. (in Japanese)

Chen, W. F. 1982. Plasticity in Reinforced Concrete. McGraw-Hill Book Company

Fuji, S. & Morita, S. 1983. Splitting bond capacities of deformed bars. *Transactions of the architectural institute of Japan* (AIJ) No.324: 45-53 (in Japanese)

Maeda, M. & Otani, S. 1994. An equation for bond splitting strength based on bond action between deformed bars and concrete. *Summaries of technical papers of annual meeting*, AIJ, Structures II: 655-658 (in Japanese)

Richart, F.E., Brandtzaeg, A. & Brown, R. L. 1928. A Study of the Failure of Concrete under Combined Compressive Stresses. Univ. of Illinois, *Engineering Experiment Station*, Bulletin, No.185

Shinohara, Y. & Kaneko, M. 1999. Compressive shear behavior in fracture process zone of concrete. *Journal of Structural and Construction Engineering*, AIJ, No.525: 1-6 (in Japanese)

Shinohara, Y., Miyano, K., Watanabe, H. & Hayashi, S. 2004. Active confining effect and failure mechanism for RC columns prestressed laterally. *Journal of Structural and Construction Engineering*, AIJ, No.578: 115-121 (in Japanese)

Takamori, N., Benny Benni Assa, Nishiyama, M. & Watanabe, F. 1996. Idealization of Stress-Strain Relationship of Confined Concrete. *Proceedings of the Japan Concrete Institute*, Vol.18, No.2: 395-400 (in Japanese)

Watanabe, H., Katori, K., Shinohara, Y. & Hayashi, S. 2004. Shear crack control by lateral prestress on reinforced concrete column and evaluation of shear strength. *Journal of Structural and Construction Engineering*, AIJ, No.577: 109-116 (in Japanese)